Title

Frequency response of a fixed–fixed pipe immersed in viscous fluids, conveying internal steady flow

Authors

Kjolsing, Eric J
Todd, Michael D

Publication Date

2015-10-01

DOI

10.1016/j.petrol.2015.02.033

Peer reviewed

Frequency Response of a Fixed-Fixed Pipe Immersed in Viscous Fluids, Conveying Internal Steady Flow

Author Names and Affiliations

Eric J. Kjolsing [a], Michael D. Todd [a]

[a] *Department of Structural Engineering, University of California, San Diego, La Jolla, CA 92093, USA*

Contact Information

Eric J. Kjolsing
9500 Gilman Drive, Mail Code 0085
La Jolla, CA 92093-0085
Eric.Kjolsing@gmail.com
1-858-722-4493

Michael D. Todd (corresponding author)
9500 Gilman Drive, Mail Code 0085
La Jolla, CA 92093-0085
mdtodd@ucsd.edu
1-858-534-5951

Contributors

Eric Kjolsing contributed to the design of the study, the development of the analytical model, interpretation of data generated from the model, and the drafting of this article.

Michael Todd contributed to the conception and design of the study, interpretation of data generated from the model, and revision of this article for important intellectual content.

Both authors have reviewed and approved the final article for submission.

Role of the Funding Source

Funding was provided by Los Alamos National Laboratory through the Engineering Institute under Task 5 (Subcontract No. 77137-001-11). The funding source was not involved with study design; collection, analysis or interpretation of data; in the writing of the report; or in the decision to submit the article for publication.

Category

Full-length article.

Abstract

Novel methods are desired to harvest and store power in harsh environments, like those found at the bottom of production wells, to power commercially available monitoring devices. These systems must not only be mechanically robust but also operationally resilient, capable of sufficient power output under the widely varying conditions expected over the service life of a well. Since energy harvesting systems are heavily dependent on natural frequency, this broad range of conditions and/or well configurations makes the design of a suitable energy harvester challenging. Although the American Petroleum Institute (API) has set standards on some of the system variables, other variables are less well defined and may be time dependent. A first step towards the design of an energy harvesting system, then, is to investigate the changes in the natural frequency of a well by varying those inputs possessing moderate to high uncertainty.

An analytical model is formed using Euler-Bernoulli beam theory to model the coupled fluid-structural system found in a producing well. A hydrodynamic function is included in the formulation to model the effects of the viscous fluid filled annulus. Due to the form of the hydrodynamic function, the systems natural frequency is solved in the frequency domain using the spectral element method; a method for calculating the displacement response to an external force is also provided. A parametric study is performed to determine the effect various inputs have on a systems first natural frequency. The key inputs considered are the axial force in the production tube, the conveyed fluid velocity, and the hydrodynamic function, itself a function of the annulus fluid viscosity and geometry.

The study's results are in-line with expectations based on previous publications investigating component wise analogous systems. The inclusion of an axial force shifts the natural frequency of the system and the conveyed fluid velocity at which divergence occurs. The added mass introduced by the real part of the hydrodynamic function causes a shift in natural frequency but not in the bifurcation point. Viscous effects generated by the imaginary part of the hydrodynamic function act to shift the natural frequency of the system and the bifurcation point. Approved for publication, LA-UR-14-27597.

Keywords

- Hydrodynamic function
- Hydrocarbon production
- Spectral element method
- Dynamics
- Flow-induced vibration
- Energy harvesting

Highlights

- A production tube confined in a viscous fluid was modeled.
- A parametric study investigating axial and annulus fluid effects was performed.
- Axial compression decreases the critical velocity at which divergence occurs.
- Added mass does not change the velocity at which bifurcation occurs.
- Viscous effects change the velocity at which bifurcation occurs.

Nomenclature

Dimensional Terms

c	Viscous Damping Coefficient
d	Pipe Outer Radius
$\boldsymbol{d}$	Nodal Degrees of Freedom Vector
$\boldsymbol{d_g}$	Global Spectral Nodal DOFs Vector
$\boldsymbol{f}$	Nodal Forces Vector
$\boldsymbol{f_g}$	Global Spectral Nodal Forces Vector
f_{hydro}	Hydrodynamic Force
g	Coefficient of Gravity
m	Mass per Unit Length of Pipe
m_{added}	Added Mass
$\bar{p}$	Mean Pressure Differential
t	Time
w	Lateral Deflection of the Pipe
w_t	Pipe Wall Thickness
x	Spatial Location Along Pipe
A_i	Flow Area
A_p	Pipe Cross Sectional Area
B	Coefficient
D	Confining Shell Inner Radius
E	Young's Modulus
E^*	Kelvin-Voigt Viscosity
$\hat{F}_h$	Fourier Transform of Hydrodynamic Force
I	Pipe Inertia
K	System Stiffness
L	Pipe Length
L^e	Spectral Element Length
M	Nodal Moment
M_i	Mass per Unit Length of Conveyed Fluid
P_{Euler}	Euler Buckling Load
Q	Nodal Shear
$\boldsymbol{S}$	Spectral Element Matrix
$\boldsymbol{S_g}$	Global Spectral Matrix
$\bar{T}$	Externally Applied Tension
U	Mean Axial Flow Velocity

Dimensional Terms (cont.)

U_{cr}	Critical Fluid Velocity
$U_0 e^{i\omega t}$	Pipe Velocity
$\hat{W}$	Fourier Transform of Lateral Deflection of Pipe
α	Coefficient of Thermal Expansion
ρ_e	Annulus Fluid Density
ρ_p	Pipe Density
υ_e	Annulus Fluid Kinematic Viscosity
ω	Radial Frequency
ω_i	Imaginary Part of Natural Frequency
ω_n	Natural Frequency
ω_r	Real Part of Natural Frequency
ΔT	Temperature Differential

Dimensionless Terms

i	Imaginary Unit
k	Wavenumber
u	Normalized Fluid Velocity
u_{cr}	Nondimensional Critical Fluid Velocity
$\boldsymbol{A}$	Assembly Matrix
C	Coefficient to be Determined
I_0, I_1, K_0, K_1	Modified Bessel Functions
$Im[\,]$	Imaginary Part
$Re[\,]$	Real Part
δ	Log Decrement
ν	Poisson Ratio
Γ	Hydrodynamic Function
Γ_i	Imaginary Part of the Hydrodynamic Function
$\Gamma_{inviscid}$	Hydrodynamic Function for Inviscid Case
Γ_r	Real Part of the Hydrodynamic Function
Λ	= 1 for Constrained Axial Motion
Ω	Normalized Natural Frequency
Ω_c	Normalized Natural Frequency Adjusted for Compression

1. Introduction

Engineers are often interested in the dynamic behavior of systems. In the case of production strings, engineers may be concerned with the accumulation of cyclic fatigue damage, dynamic effects on in-line components, or vibration induced impacts (all of which may result in well downtime). Engineers may also be interested in the dynamic behavior of a production string for a more beneficial purpose: a source of power for downhole equipment.

Well monitoring systems are often deployed on production strings to facilitate optimal hydrocarbon extraction. Ideally, these systems would be powered locally by energy harvested from and stored adjacent to the system. This, in combination with commercially available acoustic telemetry systems, may reduce or eliminate the need for running conductor cable within the annulus from surface to reservoir. Of the types of energy available for harvesting, mechanical vibration stemming from the kinetic energy of the produced fluid appears to be the most convenient. However, a wide range of environmental and production conditions could exist over the service life of a given well, making the task of estimating the frequency and amplitude of vibrations, and indirectly the harvestable energy, difficult. If the harvesting system is to be commercially viable and thus deployable on a wide variety of wells, the range of values taken on by the variables of interest increases, making the task more challenging.

Since energy harvesting systems are frequency-dependent with production generally optimized when operating at a fundamental frequency, it is pertinent to investigate the effects specific variables have on the natural frequency of the coupled fluid-structural system. Of particular interest are those variables whose values may appreciably change during the wells service life (i.e., axial force) or whose effects are not transparent (i.e., annulus fluid effects). While axial force effects in a structural system are well understood (Bokaian, 1990, 1988), there is less literature available on the effects that a viscous annulus fluid has on the natural frequency of a fluid-conveying pipe.

Significant work has been done investigating the behavior of pipes conveying fluid (Dodds and Runyan, 1965; Housner, 1952; Long, 1955; Naguleswaran and Williams, 1968), with special interest in cantilever pipes (Gregory and Paidoussis, 1966a, 1966b) due to their non-conservative nature. Other work investigating the effects of nonlinear terms (Lee and Chung, 2002) and unsteady flow (Lee et al., 1995; Lee and Park, 2006; Paidoussis and Issid, 1974; Seo et al., 2005) in similar systems can also be found. However, these research efforts do not account for the possibility of a medium external to the pipe, such as a surrounding fluid or viscoelastic foundation, which may affect the dynamics of the system. When a viscoelastic foundation is included in the system model (Hosseini et al., 2014; Lee et al., 2009; Lottati and Kornecki, 1968; Soltani et al., 2010), some of the resulting behavior may be extrapolated to the configuration of interest; however, the problem formulation is fundamentally different with the clearest manifestation being the viscoelastic foundation models failure to account for changing inertial effects. Such shortcomings become relevant since the dynamic behavior of beams vibrating in a viscous fluid is known to be altered due to both added mass and viscous effects (Sinyavskii et al., 1980; Tuck, 1969; Yeh and Chen, 1978).

The problem has been approached using a shell formulation where the treatment of inviscid fluid (Paidoussis et al., 1984), viscous fluid flow (Paidoussis et al., 1985), and the determination of added mass and damping terms (Yeh and Chen, 1977) can be found in the literature. These formulations tend to be more complicated due to the use of the shell equation of motion which permits the inclusion of additional modes beyond those produced by a beam formulation. Conveniently, for typical production tube geometries where the effective pipe length is much larger than the pipe radius, the dynamic behavior of the two formulations converge (Paidoussis, 1975). Thus, for the application of interest, a beam formulation is not only plausible but preferred as its use allows further simplification of the problem since the effects of viscous friction from the conveyed fluid vanish from the equation of motion in a beam formulation (Paidoussis, 1998).

This paper investigates the axial force effects and the effect a confined viscous fluid has on the first natural frequency of a pipe conveying fluid. Specifically, a parametric study is performed exploring the effects of axial force, annulus geometry, annulus fluid density, and annulus fluid viscosity as the conveyed fluid velocity is increased. This investigation is accomplished by forming an equation of motion based on Euler-Bernoulli beam theory that incorporates a hydrodynamic forcing term that includes both inertial and viscous effects from the annulus fluid. The problem is solved using the spectral element method (SEM), which provides a convenient approach for determining the frequency response of a given system and, if desired, its displacement response to an arbitrary forcing function. This task is undertaken so that those variables affecting the natural frequency of a subsurface length of pipe can be better understood. The presented results will be of interest to engineers working to develop an energy harvesting system for downhole deployment, as well as practicing engineers concerned with damage stemming from system dynamics.

Section 2 describes the condensation of a producing well into an analytical model. Section 3 will introduce the equation of motion, frame the problem using the spectral element method, and discuss the solution methodology while Section 4 will present the findings from the parametric study and notable observations.

2. Mapping downhole configurations to an analytical model

There is no standard configuration for a hydrocarbon well. For each producing well, a specific configuration is selected by a petroleum engineer based on the particular site and reservoir characteristics. The initial production string configuration may even vary over time as ambient temperature, fluid properties, or production string components can change over the wells service life. It is not computationally feasible to account for the broad variability or address all of the resulting effects on the dynamics of the system in a meaningful way. Accounting for the possible non-linear boundary conditions (stemming from inherent multi-axis well deviations) alone could fill a textbook. To produce meaningful results that can be generally interpreted by engineers, the wide range of possible conditions must be limited and then idealized in order to permit a reasonably sized analytical model.

The general structure of a vertical well is shown in Figure 1 (deviated wells are not investigated here). The region of interest is above and adjacent to the in-line components (monitoring systems, control

valves, etc.) that would require power generated by a deployed energy harvester. In this region, the coaxial casing and grout provide a rigid boundary which encases the annulus fluid and production string; the production string will generally consist of lengths of API standardized tubing and couplings which may vary in form. Analytically, the annulus fluid is incorporated into the model as a stagnant single-phase fluid requiring a density and viscosity input; the casing is modeled as a fixed boundary. Assuming the coupling joints result in only slight stiffness anomalies, the production tube is modeled as a constant cross section. The tubes mass can be modified in the spectral element model (described in Section 3) to account for arbitrary mass distributions caused by the joints, as desired.

The conveyed fluid produced by an operating well may range from single-phase to a multiphase flow consisting of bubble, slug, transition, or mist flow. Although multiphase fluid flow is common in oil wells, predicting its behavior is complicated due to complex heat and mass transfer through the system (Brill, 2010). Since the primary interest of this paper is the effects the annulus (annulus geometry, annulus fluid density, and annulus fluid viscosity) has on the system, the inclusion of multiphase flow in the analytical model is unnecessarily burdensome; the produced fluid, which is expected to be turbulent, is modeled as a plug flow with either average viscous or inviscid characteristics.

The last simplification made is to the boundary conditions of the production tube. In operating wells, the production tube is not likely to be centered in the well: inherent multi-axis deviation is common in the wellbore resulting in randomly located points of contact between the production tube and the production casing. This makes a neat boundary condition impossible to implement. However, the purpose of this paper is to investigate the frequency response of the system with an eye towards deploying an energy harvester and storage element along the production string. To maximize the energy that could be harvested, resonant transverse displacement of the system is desired. This resonance can be achieved through internal pressure oscillations controlled mechanically along the production string resulting in amplified translational pipe displacements. To protect the in-line components typically deployed (see Figure 1) from excessive vibrations and impacts, leading to premature fatigue failure or other damage, the length of pipe vibrating in resonance should be isolated. It is expected that the length of pipe containing the yet to be designed energy harvester will have two spaced bracing elements (see Figure 2) to prevent translation of the pipe and dampen any amplified vibrations from being transmitted to adjacent equipment. This would result in a real-world boundary condition somewhere between pinned-pinned and fixed-fixed (with the production tube itself acting to prevent rotation). Since many variables go into determining the rotational stiffness of the system (the distance between pipe/casing contact points for instance) it is best to take a bounded approach and use the neat boundary conditions available. Although the spectral element method provides a simple way to deploy various boundary conditions, this paper only focuses on the fixed-fixed condition for simplicity with the expectation that trends in the systems natural frequency found in the parametric study will be similar for the pinned-pinned case, or any elastic boundary condition case in between these extremes.

It is worth re-mentioning that the goal of this paper is to investigate the axial force effects and the effect a confined viscous fluid has on the first natural frequency of a pipe conveying fluid through a parametric study. The above assumptions are made to permit a reasonably sized analytical model while still representing the fundamental physics of the system. By capturing the fundamental physics in the model

formulation, the modeling approach and solution technique proposed in the following section can be used by petroleum engineers on specific wells of interest, thereby generating specific, rather than parametric, results.

3. Theory

Assuming small lateral motions, the linearized equation of motion for a pipe conveying fluid was derived (Paidoussis and Issid, 1974) as

$$\left(E^*\frac{\partial}{\partial t}+E\right)I\frac{\partial^4 w}{\partial x^4}+\left\{M_iU^2-\bar{T}+\bar{p}A_i(1-2\nu\Lambda)-\left[(M_i+m)g-M_i\frac{dU}{dt}\right](L-x)\right\}\frac{\partial^2 w}{\partial x^2}+ 2M_iU\frac{\partial^2 w}{\partial x\partial t}+(M_i+m)g\frac{\partial w}{\partial x}+c\frac{\partial w}{\partial t}+(M_i+m)\frac{\partial^2 w}{\partial t^2}=0, \quad (1)$$

with the general configuration given in Figure 3. The forces represented, starting with the first term, are the flexural restoring force incorporating a Kelvin-Voigt type internal dissipation effect, centrifugal force, externally applied tension force, pressure induced tension, gravity induced tension, unsteady fluid effects, Coriolis force, gravity, external viscous damping, and inertia. This equation is valid for inviscid as well as viscous conveyed fluid as explained by Paidoussis (1998).

The governing equation (1) can be generalized by including thermal and annulus fluid effects. For simplicity, the gravity-induced tension effect is dropped, and the fluid flow is taken as steady (i.e., $\frac{dU}{dt}=0$). The governing equation is then re-written as

$$E^*I\dot{w}''''+EIw''''+\left\{M_iU^2-\bar{T}+\bar{p}A_i(1-2\nu)+EA_p\alpha\Delta T\right\}w''+2M_iU\dot{w}'+ (M_i+m)gw'+c\dot{w}+(M_i+m)\ddot{w}-f_{hydro}=0, \quad (2)$$

where prime indicates a derivative with respect to x, dot indicates a derivative with respect to time and f_{hydro} is the hydrodynamic force generated by the annulus fluid effects. The general form of the hydrodynamic forcing was derived by Wamsganss et al. (1974) with similar derivations given by Stokes (1851) and Rosenhead (1963); it can be written as

$$f_{hydro}=-i\rho_e\pi d^2\omega\Gamma U_0e^{i\omega t}, \quad (3)$$

where the hydrodynamic function, Γ, is provided in Appendix A and is generally complex. If the hydrodynamic function is rewritten as $\Gamma=\Gamma_r-i\Gamma_i$, Γ_r acts to increase the effective mass of the system by contributing an added mass of $\rho_e\pi d^2\Gamma_r$ while Γ_i contributes a viscous drag term that is proportional to the pipe velocity (Cranch et al., 2013).

Noting the hydrodynamic forcing's dependence on ω both through the hydrodynamic function and the direct forcing itself, it is convenient to operate in the frequency domain where the hydrodynamic forcing is written as

$$\hat{F}_h(x|\omega) = \rho_e \pi d^2 \omega^2 \Gamma \widehat{W}(x|\omega). \tag{4}$$

Sader (1998) solved a significantly simplified version of Eq. (1) by using a Green's Function approach in the frequency domain. However, for the expanded equation of interest here, a Green's Function approach was found to be computationally expensive. Instead, a spectral element formulation approach is used. The spectral element method (SEM) solves the continuous governing equation of motion in the frequency domain as outlined in the following steps. Additional discussion of the SEM can be found in the works of Doyle (1989) and Lee (2009).

To implement the SEM, the governing equation of motion is transformed into the Fourier domain by taking the Fourier transform of Eq. (2)

$$\begin{aligned}\{(i\omega E^* + E)I\}\widehat{W}'''' + \left\{M_i U^2 - \bar{T} + \bar{p}A_i(1-2\nu) + EA_p\alpha\Delta T\right\}\widehat{W}'' + \\ \{2i\omega M_i U + (M_i + m)g\}\widehat{W}' + \{i\omega c - (M_i + m)\omega^2 - \rho_e \pi d^2 \omega^2 \Gamma\}\widehat{W} = 0.\end{aligned} \tag{5}$$

Assuming the general solution of Eq. (5) to be

$$\widehat{W} = Ce^{ikx}, \tag{6}$$

where *C* is constant and *k* is the wavenumber, and substituting Eq. (6) into Eq. (5) results in the following dispersion relation

$$\begin{aligned}\{(i\omega E^* + E)I\}k^4 - \left\{M_i U^2 - \bar{T} + \bar{p}A_i(1-2\nu) + EA_p\alpha\Delta T\right\}k^2 \\ + \{2i\omega M_i U + (M_i + m)g\}ik + \{i\omega c - (M_i + m)\omega^2 - \rho_e \pi d^2 \omega^2 \Gamma\} = 0.\end{aligned} \tag{7}$$

Equation (7) may be solved for the four wavenumbers (k_r, *r*=1…4), each a function of ω, allowing for Eq. (6) to be rewritten as

$$\widehat{W} = \sum_{r=1}^{4} C_r e^{ik_r x} = \boldsymbol{eC}, \tag{8}$$

where

$$\begin{aligned}\boldsymbol{e} &= \left\{e^{ik_1 x}\ e^{ik_2 x}\ e^{ik_3 x}\ e^{ik_4 x}\right\}, \\ \boldsymbol{C} &= \{C_1, C_2, C_3, C_4\}.\end{aligned} \tag{9}$$

Considering a single spectral element, the nodal degrees of freedom and force vectors can be written as

$$\begin{aligned}\boldsymbol{d} &= \{W_1, \Theta_1, W_2, \Theta_2\} = \left\{\widehat{W}(0), \widehat{W}'(0), \widehat{W}(L^e), \widehat{W}'(L^e)\right\}, \\ \boldsymbol{f} &= \{Q_1, M_1, Q_2, M_2\} = \{Q(0), -M(0), -Q(L^e), M(L^e)\},\end{aligned} \tag{10}$$

corresponding to the convention given in Figure 4.

Plugging Eqs. (8) and (9) into Eq. (10), a relation between the nodal degrees of freedom vector and constants vector can be established as

$$\boldsymbol{d} = \{\widehat{W}(0), \widehat{W}'(0), \widehat{W}(L^e), \widehat{W}'(L^e)\} = \{\boldsymbol{e}(0), \boldsymbol{e}'(0), \boldsymbol{e}(L^e), \boldsymbol{e}'(L^e)\}\boldsymbol{C} = \boldsymbol{HC}, \tag{11}$$

where $\boldsymbol{H}$ can be written as

$$\boldsymbol{H} = \begin{bmatrix} 1 & 1 & 1 & 1 \\ ik_1 & ik_2 & ik_3 & ik_4 \\ e^{ik_1L^e} & e^{ik_2L^e} & e^{ik_3L^e} & e^{ik_4L^e} \\ ik_1e^{ik_1L^e} & ik_2e^{ik_2L^e} & ik_3e^{ik_3L^e} & ik_4e^{ik_4L^e} \end{bmatrix}. \tag{12}$$

Considering the force vector $\boldsymbol{f}$ in Eq. (10) and noting the force relations in the spectral domain (Lee and Oh, 2003) to be

$$\begin{aligned} Q &= (i\omega E^* + E)I\widehat{W}''' - \bar{T}\widehat{W}', \\ M &= (i\omega E^* + E)I\widehat{W}'', \end{aligned} \tag{13}$$

Eqs. (8), (9), and (13) may be inserted into the force vector in Eq. (10), arriving at

$$\boldsymbol{f} = \{Q(0), -M(0), -Q(L^e), M(L^e)\} = \boldsymbol{XC}, \tag{14}$$

where $\boldsymbol{X}$ may be written as

$$\boldsymbol{X} = \begin{bmatrix} g_1 & g_2 & g_3 & g_4 \\ -h_1 & -h_2 & -h_3 & -h_4 \\ -g_1e^{ik_1L^e} & -g_2e^{ik_2L^e} & -g_3e^{ik_3L^e} & -g_4e^{ik_4L^e} \\ h_1e^{ik_1L^e} & h_2e^{ik_2L^e} & h_3e^{ik_3L^e} & h_4e^{ik_4L^e} \end{bmatrix}, \tag{15}$$

where

$$\begin{aligned} g_r &= -ik_r^3(i\omega E^* + E)I - ik_r\bar{T}, \\ h_r &= -k_r^2(i\omega E^* + E)I. \end{aligned} \tag{16}$$

The $\boldsymbol{H}$ matrix of Eqs. (11) and (12) may be inverted and substituted into Eq. (14) as

$$\boldsymbol{f} = \boldsymbol{XC} = \boldsymbol{X}(\boldsymbol{H}^{-1}\boldsymbol{d}) = \boldsymbol{Sd}, \tag{17}$$

where the spectral element matrix $\boldsymbol{S}$ can be defined as

$$\boldsymbol{S} = \boldsymbol{X}\boldsymbol{H}^{-1}. \tag{18}$$

The global spectral matrix ($\boldsymbol{S_g}$) can be assembled from the spectral element matrices in a manner similar to a finite element formulation. Boundary conditions can be incorporated at this point. For instance, for a two-element fixed-fixed model (two elements are required to have a non-zero rank matrix) as shown in Figure 5, the global spectral matrix can be assembled as

$$\boldsymbol{S_g} = \boldsymbol{A_1^T S A_1} + \boldsymbol{A_2^T S A_2}, \tag{19}$$

with

$$\boldsymbol{A_1^T} = \begin{bmatrix} 0 & 0 & 1 & 0 \\ 0 & 0 & 0 & 1 \end{bmatrix}, \quad \boldsymbol{A_2^T} = \begin{bmatrix} 1 & 0 & 0 & 0 \\ 0 & 1 & 0 & 0 \end{bmatrix}. \tag{20}$$

The physical construction of the assembly process described by Eq. (19) is shown in Figure 6.

For a pinned-pinned beam, $\boldsymbol{A_1}$ and $\boldsymbol{A_2}$ are written as

$$\boldsymbol{A_1} = \begin{bmatrix} 0 & 0 & 0 & 0 \\ 1 & 0 & 0 & 0 \\ 0 & 1 & 0 & 0 \\ 0 & 0 & 1 & 0 \end{bmatrix}, \quad \boldsymbol{A_2} = \begin{bmatrix} 0 & 1 & 0 & 0 \\ 0 & 0 & 1 & 0 \\ 0 & 0 & 0 & 0 \\ 0 & 0 & 0 & 1 \end{bmatrix}. \tag{21}$$

Having applied the relevant boundary conditions, the equation of interest is then

$$\boldsymbol{f_g} = \boldsymbol{S_g d_g}. \tag{22}$$

The natural frequencies can be solved by setting the determinant of $\boldsymbol{S_g}$ to zero and solving for ω_n. For a forced dynamic response, the displacement at the free nodes can be determined by:

1. For loads applied to free DOFs, transform the nodal force into the frequency domain and assemble $\boldsymbol{f_g}$.
2. Invert $\boldsymbol{S_g}$ and solve for $\boldsymbol{d_g}$ using Eq. (22).
3. Disassemble the global response into the element response (i.e. $\boldsymbol{d_g}$ □ $\boldsymbol{d}$).
4. Calculate the $\boldsymbol{C}$ vector using Eqs. (11) and (12).
5. Calculate the frequency response $\widehat{W}$ using Eq. (8).
6. Apply an inverse Fourier transform to determine the displacement response in the time domain.

The inverse Fourier transform is done discretely to reduce computation time. The tradeoff, when compared to the continuous inverse transform, is the user must specify which frequencies to include from $\widehat{W}$ and the frequency domain sampling rate (Narayanan and Beskos, 1978).

4. Results and discussion

It is desirable to understand and characterize the effects fluid velocity, axial force, annulus geometry, and annulus fluid properties have on the systems natural frequency. A parametric study is undertaken in which the systems first natural frequency is plotted for specific variables of interest over a range of fluid velocities. Where possible, calculations are simplified by setting irrelevant variables to 0 or ∞ as appropriate. The input values used for each case are tabulated in Appendix B. The numeric values used as inputs were selected as they fall within a reasonable range for what might be found during hydrocarbon production. As the results presented are from a parametric study, the input values used are not intended to coincide with any specific value found in practice. However, a practicing engineer may generate similar results using the model outlined in the Theory section and their own numeric inputs stemming from a specific well configuration of interest.

For plotting purposes, the flow velocity and natural frequency are normalized as

$$u = \sqrt{\frac{M_i}{EI}}UL \quad , \quad \Omega = \sqrt{\frac{M_i+m}{EI}}\omega L^2. \tag{23}$$

4.1 Axial force effects

A system is subjected to three levels of axial force $\bar{T}$ = 100 kN, 0 kN and -200 kN (cases I, II and III respectively) with negative values implying compression; results are presented in Figure 7. For case II (the unloaded case) the natural frequency for zero fluid flow (22.37) and at the critical flow velocity (-6.28) match published data (Paidoussis, 1998; Rao, 2007).

Using case III (the compression case) as an illustrative example, the vertical shift in the real part of the natural frequency under zero flow compares favorably with documented results; Bolotin (1964) suggests the relation

$$\Omega_c = \Omega\sqrt{1 + \bar{T}/P_{Euler}}\,. \tag{24}$$

Noting $P_{Euler} = 550\ kN$ for the system presented, Bolotin's equation results in $\Omega_c = 17.84$ versus a calculated value of $\Omega_c = 17.96$ using the SEM method (error =0.7%). The lateral shift in the critical flow velocity relates to the applied axial force as $\bar{T} \sim M_i U^2$: the fluid velocity has the effect of inducing compression in the system. This relationship is apparent when looking at the equation of motion (1) and has been documented by Housner (1952). The critical velocity can then be calculated as $U_{cr} = \sqrt{(P_{Euler} + \bar{T})/M_i}$. In nondimensional form $u_{cr} = -5.01$, agreeing with the results presented in Figure 7.

Bifurcation of the imaginary natural frequency occurs when the real part of the natural frequency reaches zero ($Re[\Omega] = 0$). Divergence instability occurs when both the real and imaginary parts of the natural frequency reach zero ($Re[\Omega] = Im[\Omega] = 0$). Due to the Coriolis effect ($2i\omega M_i U\widehat{W}'$) and the fixed-fixed boundary condition, a small imaginary part of the natural frequency exists prior to

bifurcation (on the order of $Im[\Omega]$~0.005). Because of this, the bifurcation point and divergence point do not exactly coincide, although the difference in this case is almost undiscernible.

4.2 Annulus fluid density effects

The annulus fluid density manifests itself in the equation of motion as a multiplier of—but does not play a direct role in defining—the hydrodynamic function. It is, however, used to define the hydrodynamic force (see Eq. (3)). The annulus fluid density could then be thought of as a sort of scaling factor applied to the effects of the hydrodynamic function where for $\rho_e = 0$ the hydrodynamic function plays no role while for $\rho_e \neq 0$ hydrodynamic effects will be included.

Consider the cases presented in Table 1. The zero flow case provides a useful illustration if the discussion is restricted to inviscid systems: the effects of the annulus fluid density can be directly observed through the added mass contributed by the hydrodynamic function. For case IV, where $\rho_e = 0$, the natural frequency of the system can be calculated as $\Omega = 22.37$ ($\omega_n = 48.95\, rad/s$) where the system mass includes both the conveyed fluid and pipe mass and can be written as $M_i + m = 35.98\, kg/m$ (i.e. there is no added mass). The system stiffness can then be determined as $K = \omega_n^2(M_i + m) = 86225\, kg/ms^2$. By selecting various fluid densities and hydrodynamic functions, the shift in natural frequency due to the added mass ($\rho_e \pi d^2 \Gamma_r$) can be calculated and compared with the SEM output. Table 1 shows excellent agreement between the SEM results and the simplified method presented here.

4.3 Annulus viscosity and geometry effects

The annulus viscosity and geometry act to shape the hydrodynamic function in a complicated way (see Appendix A). Rather than trying to understand the complex link between these three variables (υ_e, *D*, *d*) and the natural frequency, it is easier to first examine the relationship between these variables and the hydrodynamic function and later observe how the hydrodynamic function effects the natural frequency.

4.3.1 Hydrodynamic Function

The hydrodynamic functions for different combinations of viscosity and geometry (see Table 2) are plotted in Figure 8 where ω is taken as purely real.

Noting Figure 8, for the range of inputs considered the real part of the hydrodynamic function is dominated by effects stemming from the *D/d* ratio while changes in the annulus viscosity result in only a small offset. In general:

- $Re[\Gamma]$ and $|Im[\Gamma]|$ decrease with an increasing *D/d* ratio.
- $Re[\Gamma]$ and $|Im[\Gamma]|$ increase with increasing υ_e.

4.3.2 An Inviscid System

Taking $\upsilon_e = 0$ results in an inviscid system and a purely real hydrodynamic function with the reduced form (Wambsganss et al., 1974)

$$\Gamma_{inviscid} = \frac{1+(d/D)^2}{1-(d/D)^2}. \tag{25}$$

As previously discussed, the real part of the hydrodynamic function results in an increased system mass by generating an added mass term ($\rho_e \pi d^2 \Gamma_r$). Rewriting the inertial and hydrodynamic forcing terms from Eq. (5) makes the contribution apparent:

$$\{-(M_i + m)\omega^2 - \rho_e \pi d^2 \omega^2 \Gamma_r\}\widehat{W} = \{-(M_i + m + \rho_e \pi d^2 \Gamma_r)\omega^2\}\widehat{W}. \tag{26}$$

To illustrate the effect of added mass, three cases (VIII-X) are investigated with the SEM results plotted in Figure 9. As was done in Section 3.2, the shifts in natural frequency for zero flow velocity can be predicted analytically and compared to the SEM results. This is done in Table 3 with the results exhibiting excellent agreement between the two methods.

Lastly, since divergence is a static phenomenon its occurrence is not dependent on inertial effects meaning the addition of added mass does nothing to change the critical flow velocity, as illustrated in Figure 9 which shows all three cases converging to the same critical flow velocity ($u = -6.28$). The added mass, however, does effect post-divergence frequencies as is apparent in the plot of imaginary natural frequencies.

4.3.3 A Viscous System

Four cases (XI-XIV) are analyzed to observe the effects the full hydrodynamic function has on the system (i.e., $v_e \neq 0$). The resulting normalized fluid velocity vs. normalized frequency curves are shown in Figure 10.

Unlike the inviscid case, the vertical shift in $Re[\Omega]$ is now due to both added mass (contributed by the real part of the hydrodynamic function) and viscous drag (contributed by the imaginary part of the hydrodynamic function). Figure 10 indicates that the real part of the natural frequencies for cases XII and XIII at zero flow velocity nearly coincide (10.10 vs. 9.90). However, the added mass generated by the specific configuration of case XII is nearly 65% greater than that in case XIII. If viscous effects were not acting to shift the natural frequencies one would expect $Re[\Omega]$ for case XII to be lower than that of case XIII (recalling that an increase in added mass acts to lower $Re[\Omega]$). However, case XIII has significantly more viscous drag ($\Gamma_{i;\,case\ XIII}/\Gamma_{i;\,case\ XII} = 3.7$) which acts to decrease the natural frequency, a characteristic of damping that is widely known, and results in the closely spaced natural frequencies shown.

To confirm the results of Figure 10 and to illustrate the SEMs capability in producing displacement results the free vibration response for case XII was determined using the method outlined in Section 2. While taking $U = 0$, a point force was applied at midspan and then removed at t = 15 sec. The midspan free vibration response was then plotted as shown in Figure 11. A Laplace Transform was taken of the time history output to confirm the real and imaginary parts of the natural frequency given in Figure 10. If the form of the response is assumed to be defined by a decaying exponential (i.e., $w(t) =$

$BCos[\omega_r t]e^{-\omega_i t}$), then it is clear that the real part of the natural frequency ($\omega_r = Re[\omega]$) corresponds to the frequency of vibration while the imaginary part ($\omega_i = Im[\omega]$) to the decay rate.

As the flow rate increases, $Re[\Omega]$ approaches zero. Using the just defined decaying exponential equation, the log decrement can be calculated as

$$\delta = ln\left(\frac{A}{Ae^{-2\pi(\omega_i/\omega_r)}}\right) = 2\pi\frac{\omega_i}{\omega_r} \tag{27}$$

so that as $Re[\Omega]$ approaches zero (and noting that $Im[\Omega]$ is relatively constant prior to bifurcation) the equivalent viscous damping increases from its case specific initial value to critical damping at bifurcation (a trend noted by Dodds and Runyan (1965)). After bifurcation but prior to divergence, the system acts in an overdamped fashion in which oscillation does not occur ($Re[\Omega] = 0$) but the system remains stable ($Im[\Omega] > 0$). Once divergence has occurred (i.e., $Re[\Omega] = Im[\Omega] = 0$) the system becomes unstable, and since divergence is a static phenomenon that is independent of damping, the critical velocities for all four cases converge to $u_{cr} = -6.28$.

Although the point of divergence has not changed, the velocity at which bifurcation occurs has shifted between the four cases. Understanding that this shift is not due to added mass (as laid out in Section 3.3.2) it must be due to the inclusion of viscous drag effects. Graphically, turning to the $Im[\Omega]$ plot of Figure 10, the necessity of this shift stems from the existence of a positive imaginary component of the natural frequency prior to bifurcation and the requirement that the point of divergence for all four cases coincide. This shift of the bifurcation point due to viscous effects has been previously demonstrated in the literature (Hosseini et al., 2014; Soltani et al., 2010).

Lastly, it should be noted that once the system becomes unstable the results presented here may become questionable, as the linearization assumptions used to define the hydrodynamic function may no longer be valid.

5. Conclusions

Using Euler-Bernoulli beam theory, the spectral element method was used to determine the frequency response of a pipe conveying fluid, confined by an external viscous fluid. The formulation permits any number of variables to be parametrically investigated, allowing practicing engineers the opportunity to re-create the current study with their own specific inputs from a specific well configuration of interest. For the current study, the variables of interest were the axial force in the system, conveyed fluid velocity, annulus fluid properties, and annulus geometry. The following results were found: Shifts in the natural frequencies due to axial load match previously published findings. The annulus fluid density acts to scale the effect of the hydrodynamic function, in turn defining the hydrodynamic force. The effects of the hydrodynamic function are driven by the annulus fluid viscosity and annulus geometry. The real part of the hydrodynamic function contributes additional mass to the system, which causes a shift in the systems natural frequency but not in the velocity at which bifurcation occurs. The imaginary part of the hydrodynamic function acts to both shift the natural frequency of the system and the velocity at which

bifurcation occurs. These findings give insight into the dynamic behavior of a submerged pipe conveying fluid, like what might be found in a hydrocarbon producing well, and would be of interest to engineers developing a mechanically based downhole energy harvesting system or those concerned by damage stemming from system vibration.

6. Acknowledgments

Funding was provided by Los Alamos National Laboratory through the Engineering Institute under Task 5 (Subcontract No. 77137-001-11). The funding source was not involved with study design; collection, analysis or interpretation of data; in the writing of the report; or in the decision to submit the article for publication.

Appendix A

The hydrodynamic force is written as

$$f_{hydro} = -i\rho_e \pi d^2 \omega \Gamma U_0 e^{i\omega t}, \tag{A.1}$$

where the hydrodynamic function can be written as

$$\Gamma = \frac{\Gamma_{num}}{\Gamma_{den}} - 1 = Re[\Gamma] - iIm[\Gamma], \tag{A.2}$$

with

$$\begin{aligned}\Gamma_{num} = {} & 2\alpha^2[I_0(\alpha)K_0(\beta) - I_0(\beta)K_0(\alpha)] - 4\alpha[I_1(\alpha)K_0(\beta) + I_0(\beta)K_1(\alpha)] \\ & + 4\alpha\gamma[I_0(\alpha)K_1(\beta) + I_1(\beta)K_0(\alpha)] - 8\gamma[I_1(\alpha)K_1(\beta) - I_1(\beta)K_1(\alpha)],\end{aligned} \tag{A.3}$$

$$\begin{aligned}\Gamma_{den} = {} & \alpha^2(1-\gamma^2)[I_0(\alpha)K_0(\beta) - I_0(\beta)K_0(\alpha)] \\ & + 2\alpha\gamma[I_0(\alpha)K_1(\beta) - I_1(\beta)K_0(\beta) + I_1(\beta)K_0(\alpha) - I_0(\beta)K_1(\beta)] \\ & + 2\alpha\gamma^2[I_0(\beta)K_1(\alpha) - I_0(\alpha)K_1(\alpha) + I_1(\alpha)K_0(\beta) - I_1(\alpha)K_0(\alpha)].\end{aligned}$$

The arguments to the hydrodynamic function are

$$\bar{k} = \sqrt{\frac{i\omega}{\upsilon_e}}; \quad \alpha = \bar{k}d; \quad \beta = \bar{k}D; \quad \gamma = \frac{d}{D}. \tag{A.4}$$

Assumptions used in the derivation of the hydrodynamic function are included in Table A.1.

Appendix B

The inputs used in the various cases are provided in Table B.1.

References

Bokaian, A. "Natural frequencies of beams under tensile axial loads." *Journal of Sound and Vibration* 142.3 (1990): 481-498.

Bokaian, A. "Natural frequencies of beams under compressive axial loads." *Journal of Sound and Vibration* 126.1 (1988): 49-65.

Bolotin, V. V. *The dynamic stability of elastic systems*. Holden− Day, lnc., 1974.

Brill, J. "Modeling Multiphase Flow in Pipes," *Society of Petroleum Engineers: The Way Ahead* 6.2 (2010): 16-17.

Cranch, G. A., Lane, J. E., Miller, G. A. and Lou, J. W., "Low frequency driven oscillations of cantilevers in viscous fluids at very low Reynolds number." *Journal of Applied Physics* 113.19 (2013): 194904.

Dodds Jr, H. L. and Runyan, H. L. “Effect of high-velocity fluid flow on the bending vibrations and static divergence of a simply supported pipe.” No. NASA-TN-D-2870. National Aeronautics and Space Administration Hampton VA Langley Research (1965).

Doyle, J. F. *Wave propagation in structures*. Springer US, 1989.

Gregory, R. W. and Paidoussis, M. P. "Unstable oscillation of tubular cantilevers conveying fluid. I. Theory." *Proceedings of the Royal Society of London. Series A. Mathematical and Physical Sciences* 293.1435 (1966): 512-527.

Gregory, R. W. and Paidoussis, M. P. "Unstable oscillation of tubular cantilevers conveying fluid. II. Experiments." *Proceedings of the Royal Society of London. Series A. Mathematical and Physical Sciences* 293.1435 (1966): 528-542.

Hosseini, M., Sadeghi-Goughari, M., Atashipour, S. A., and Eftekhari, M. "Vibration analysis of single-walled carbon nanotubes conveying nanoflow embedded in a viscoelastic medium using modified nonlocal beam model." *Archives of Mechanics* 66.4 (2014): 217-244.

Housner, G. W. "Bending vibrations of a pipe line containing flowing fluid." *Journal of Applied Mechanics-Transactions of the ASME* 19.2 (1952): 205-208.

Lee, S. I. and Chung, J. "New non-linear modelling for vibration analysis of a straight pipe conveying fluid." *Journal of Sound and Vibration* 254.2 (2002): 313-325.

Long, R. H. "Experimental and theoretical study of transverse vibration of a tube containing flowing fluid." *Journal of Applied Mechanics* 77.1 (1955): 65-68.

Lee, U. *Spectral element method in structural dynamics*. John Wiley & Sons, 2009.

Lee, U. and Oh, H. "The spectral element model for pipelines conveying internal steady flow." *Engineering structures* 25.8 (2003): 1045-1055.

Lee, U., Jang, I., and Go, H. "Stability and dynamic analysis of oil pipelines by using spectral element method." *Journal of Loss Prevention in the Process Industries* 22.6 (2009): 873-878.

Lee, U., Pak, C. H., and Hong, S. C. "The dynamics of a piping system with internal unsteady flow." *Journal of Sound and Vibration* 180.2 (1995): 297-311.

Lee, U. and Park, J. "Spectral element modelling and analysis of a pipeline conveying internal unsteady fluid." *Journal of Fluids and Structures* 22.2 (2006): 273-292.

Lottati, I. and Kornecki, A. "The effect of an elastic foundation and of dissipative forces on the stability of fluid-conveying pipes." *Journal of Sound and Vibration* 109.2 (1986): 327-338.

Naguleswaran, S. and Williams, C. J. H. "Lateral vibration of a pipe conveying a fluid." *Journal of Mechanical Engineering Science* 10.3 (1968): 228-238.

Narayanan, G. V. and Beskos, D. E. "Use of dynamic influence coefficients in forced vibration problems with the aid of fast Fourier transform." *Computers & Structures* 9.2 (1978): 145-150.

Paidoussis, M. P. *Fluid-structure interactions: slender structures and axial flow*. Vol. 1. Academic press, 1998.

Paidoussis, M. P. "Flutter of conservative systems of pipes conveying incompressible fluid." *Journal of Mechanical Engineering Science* 17.1 (1975): 19-25.

Païdoussis, M. P., Chan, S. P. and Misra, A. K. "Dynamics and stability of coaxial cylindrical shells containing flowing fluid." *Journal of Sound and Vibration* 97.2 (1984): 201-235.

Paidoussis, M. P. and Issid, N. T. "Dynamic stability of pipes conveying fluid." *Journal of Sound and Vibration* 33.3 (1974): 267-294.

Païdoussis, M. P., Misra, A. K., and Chan, S. P. "Dynamics and stability of coaxial cylindrical shells conveying viscous fluid." *Journal of Applied Mechanics*52.2 (1985): 389-396.

Rao, S. S. *Vibration of continuous systems*. John Wiley & Sons, 2007.

Rosenhead, L. *Laminar Boundary Layers*. Oxford: Clarendon Press, 1963.

Sader, J. E. "Frequency response of cantilever beams immersed in viscous fluids with applications to the atomic force microscope." *Journal of Applied Physics* 84.1 (1998): 64-76.

Seo, Y. S., Jeong, W. B., Jeong, S. H., and Oh, J. S. "Finite element analysis of forced vibration for a pipe conveying harmonically pulsating fluid." *JSME International Journal Series C*48.4 (2005): 688-694.

Siniavskii, V. F., Fedotovskii, V. S., and Kukhtin, A. B. "Oscillation of a Cylinder in a Viscous Liquid." *Prikladnaia Mekhanika* 16 (1980): 62-67.

Soltani, P., Taherian, M. M., and Farshidianfar, A. "Vibration and instability of a viscous-fluid-conveying single-walled carbon nanotube embedded in a visco-elastic medium." *Journal of Physics D: Applied Physics* 43.42 (2010): 425401.

Stokes, G. G. *On the effect of the internal friction of fluids on the motion of pendulums*. Vol. 9. Pitt Press, 1851.

Tuck, E. O. "Calculation of unsteady flows due to small motions of cylinders in a viscous fluid." *Journal of Engineering Mathematics* 3.1 (1969): 29-44.

Wambsganss, M. W., Chen, S. S., and Jendrzejczyk, J. A. "Added mass and damping of a vibrating rod in confined viscous fluids." *NASA STI/Recon Technical Report N* 75 (1974): 10349.

Yeh, T. T. and Chen, S. S. "The effect of fluid viscosity on coupled tube/fluid vibrations." *Journal of Sound and Vibration* 59.3 (1978): 453-467.

Yeh, T. T., and Chen, S. S. "Dynamics of a cylindrical shell system coupled by viscous fluid." *The Journal of the Acoustical Society of America* 62.2 (1977): 262-270.

Figures

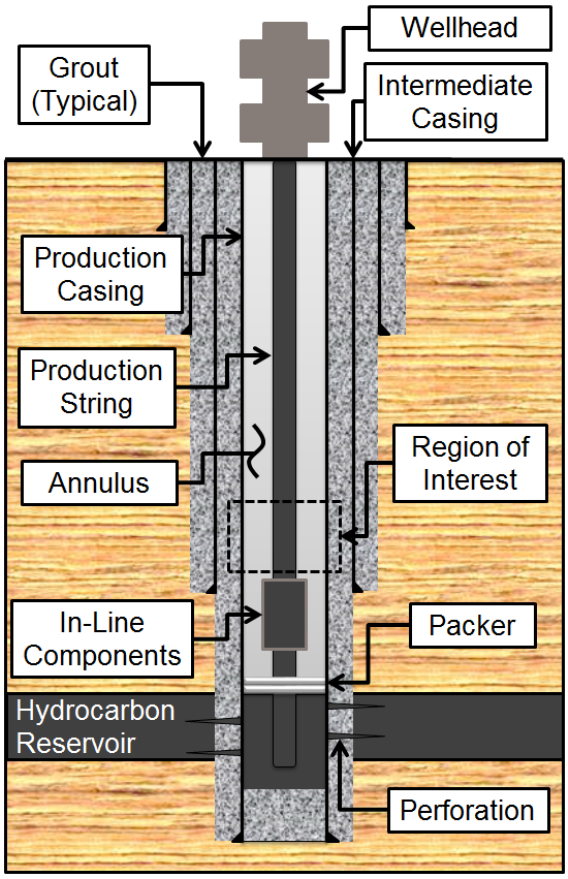

Figure 1. General Well Configuration

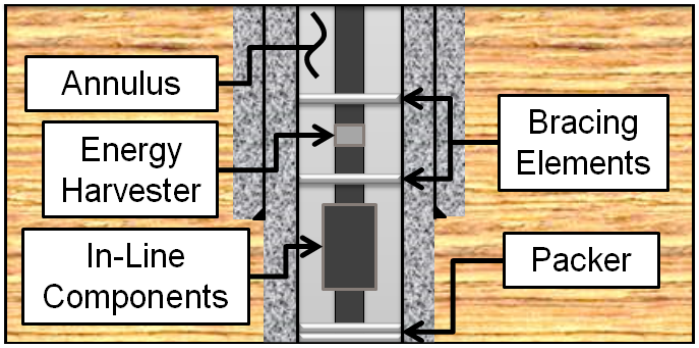

Figure 2. Modified Region of Interest

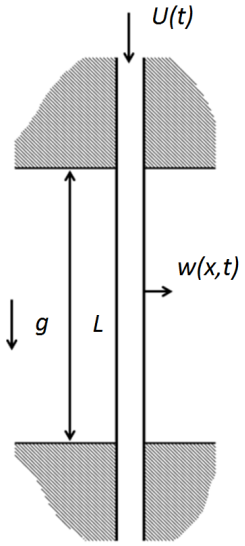

Figure 3. Model of a Pipe Conveying Internal Flow

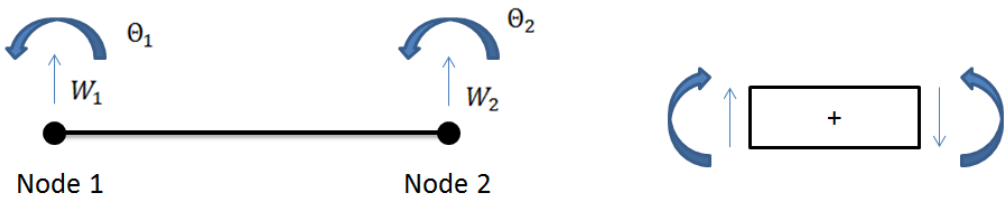

Figure 4. Element Convention: Displacement (Left) and Force (Right)

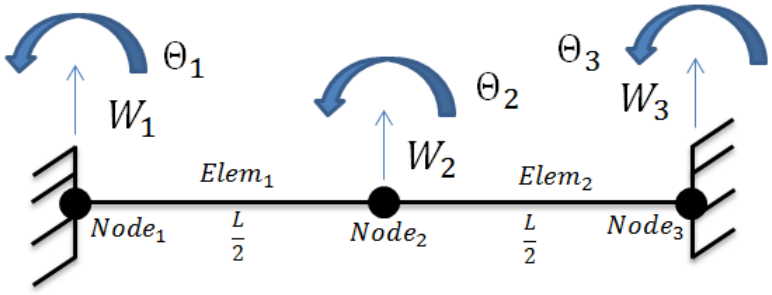

Figure 5. Two-Element Fixed-Fixed Beam Model

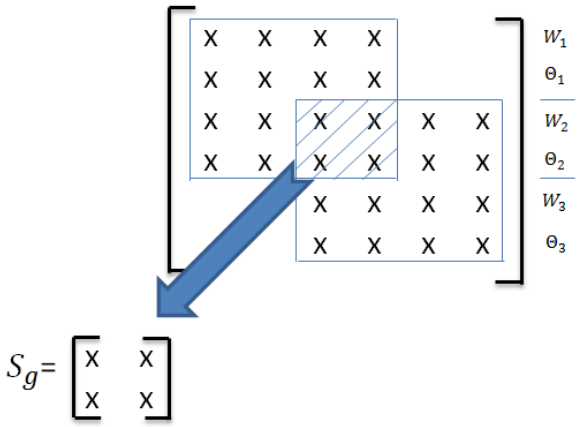

Figure 6. Global Spectral Matrix Assembly

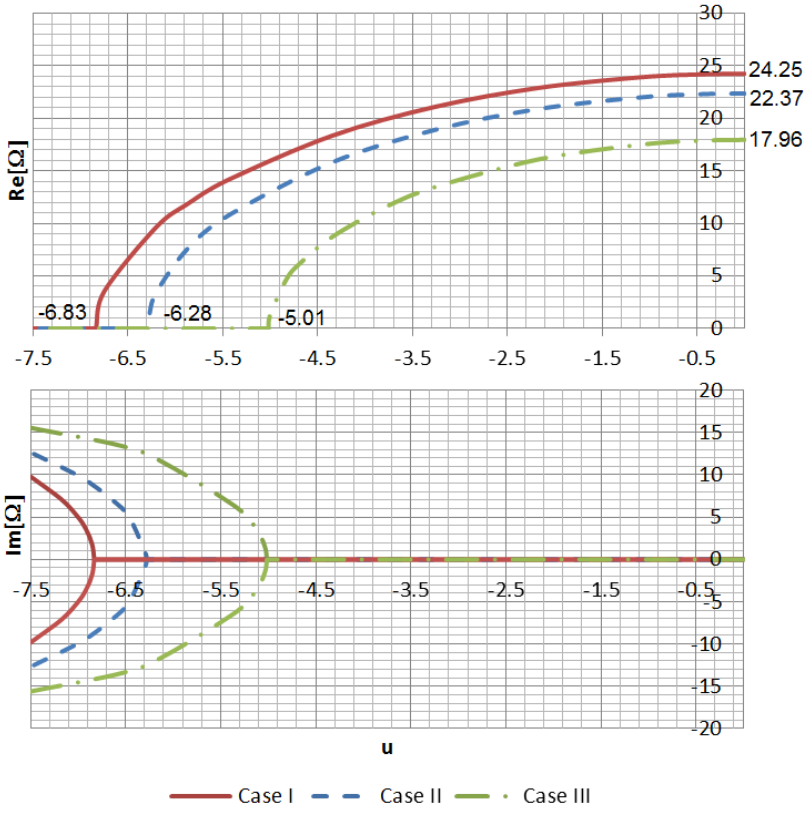

Figure 7. First Natural Frequency vs. Flow Velocity - Axial Force Effects

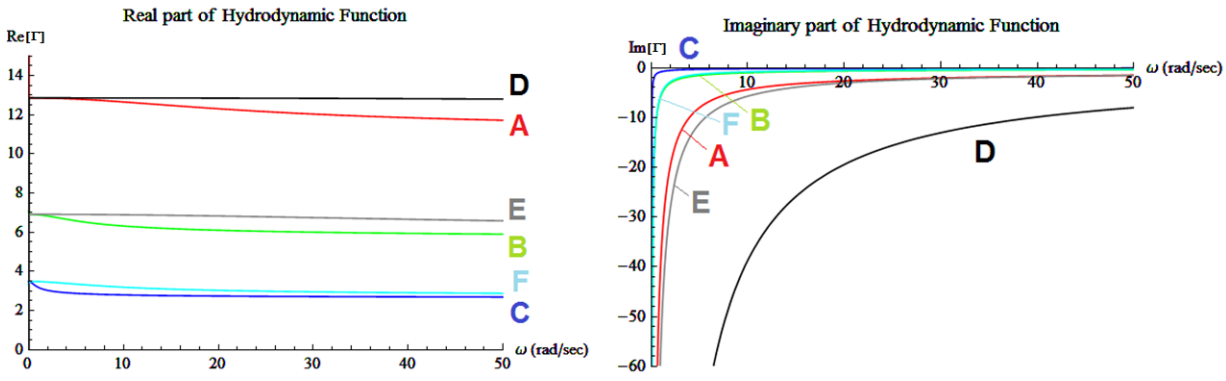

Figure 8. Hydrodynamic Functions: Left - Real Part, Right – Imaginary Part

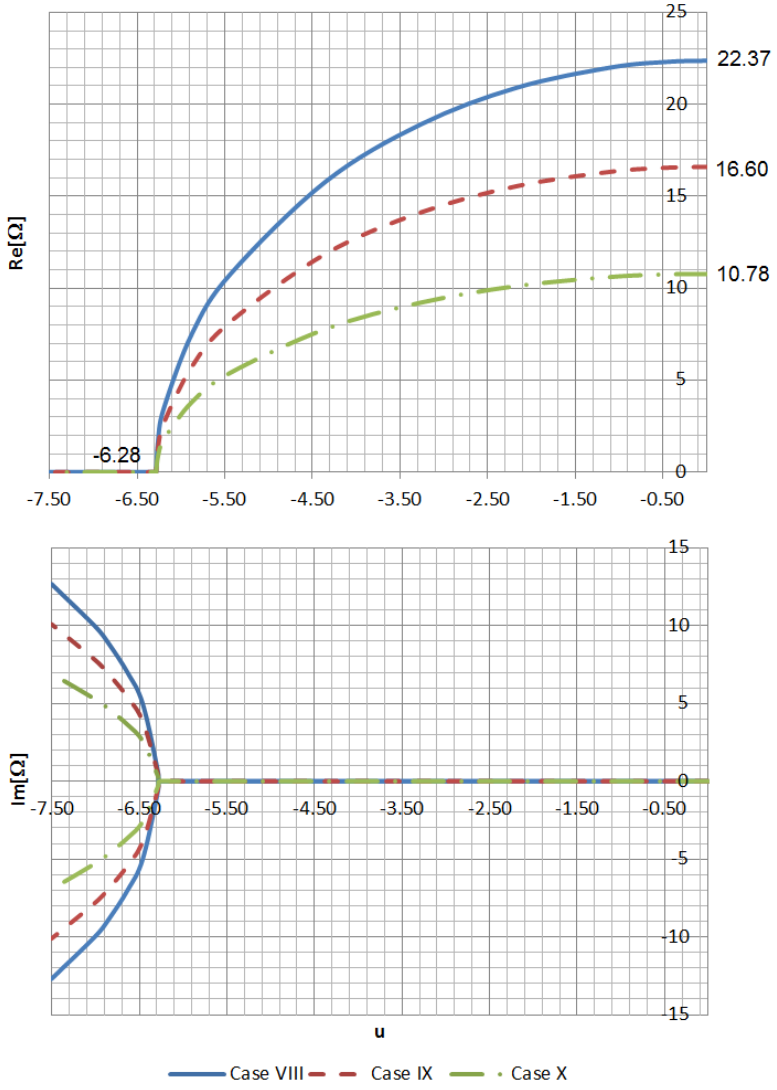

Figure 9. First Natural Frequency vs. Flow Velocity – Added Mass Effects

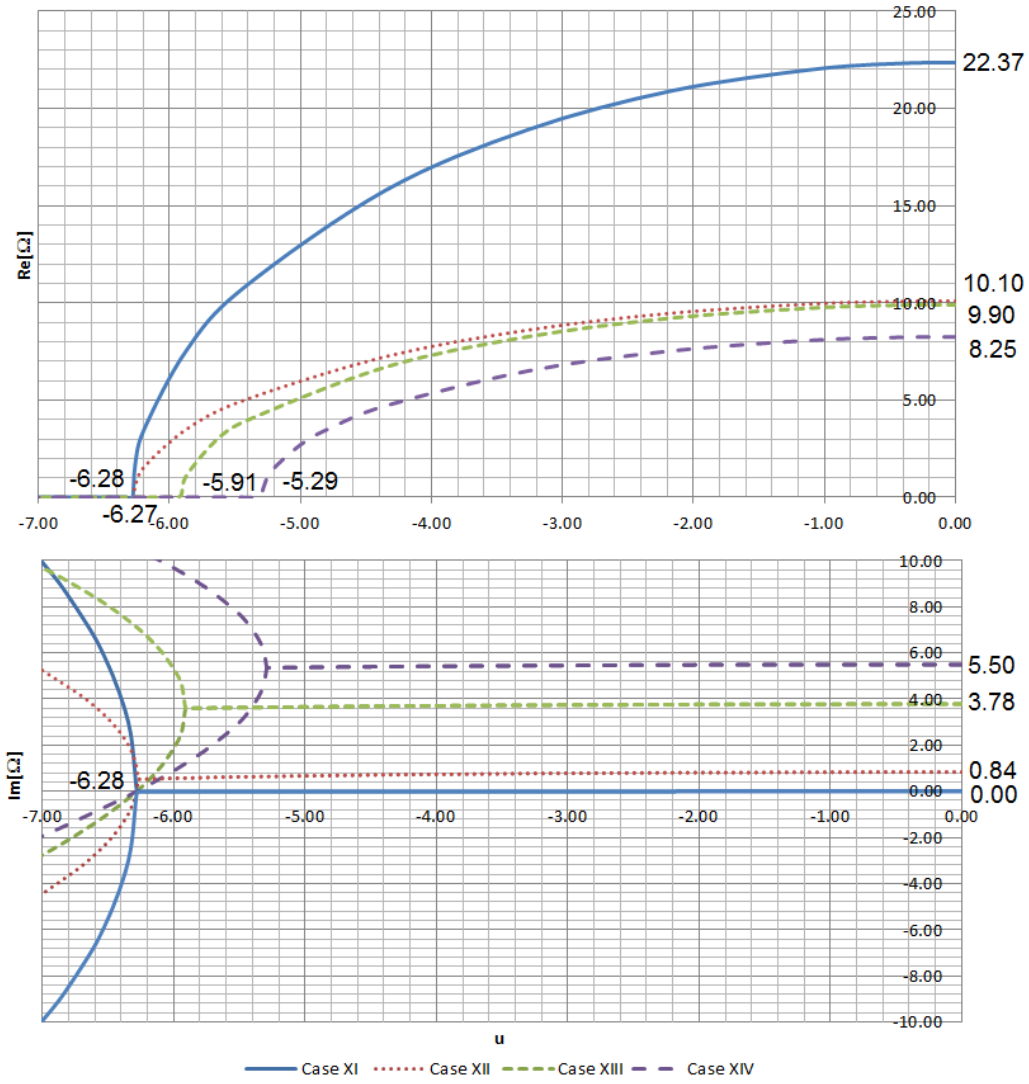

Figure 10. First Natural Frequency vs. Flow Velocity – Viscous System

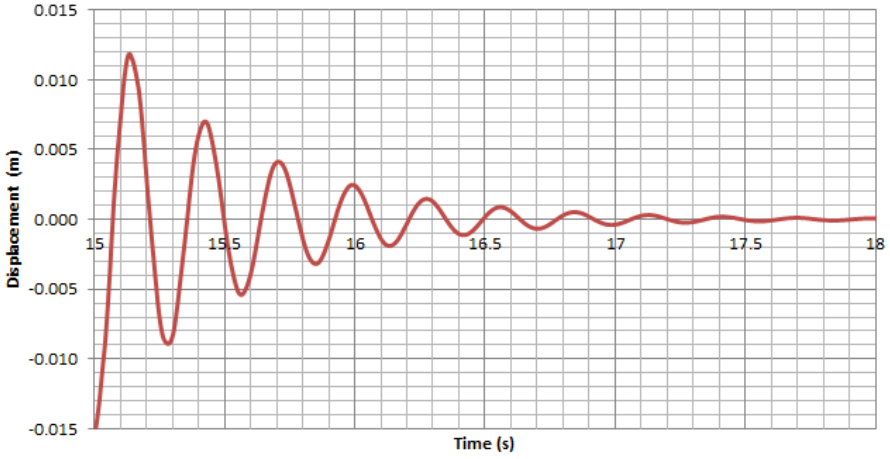

Figure 11. Free Vibration Response of Case XII

Tables

Case	Γ	$\rho_e \left(\frac{kg}{m^3}\right)$	Added Mass $\left(\frac{kg}{m}\right)$	Total Mass $\left(\frac{kg}{m}\right)$	$\omega_n\ (rad/s)$		Ω	
					Calculated*	SEM	Calculated	SEM
IV	0	0	0.00	35.98	48.95	48.95	22.37	22.37
V	1	3000	33.93	69.91	35.12	35.12	16.05	16.05
VI	2	700	15.83	51.81	40.79	40.79	18.64	18.64
VII	5	1000	56.55	92.53	30.53	30.53	13.95	13.95

* $\omega_n = \sqrt{\frac{K}{M_i + m + m_{added}}}$

Table 1. The Role of Annulus Fluid Density

		$v_e \left(\frac{m^2}{s}\right)$	
		1.00E-05	1.00E-04
$\frac{D}{d}$	1.1	A	D
	1.2	B	E
	1.5	C	F

d=0.06m

Table 2. Hydrodynamic Function Matrix

Case	Γ	$\rho_e \left(\frac{kg}{m^3}\right)$	Added Mass $\left(\frac{kg}{m}\right)$	Total Mass $\left(\frac{kg}{m}\right)$	$\omega_n\ (rad/s)$		Ω	
					Calculated*	SEM	Calculated	SEM
VIII	1.00	0	0.00	35.98	48.95	48.95	22.37	22.37
IX	2.60	1000	29.41	65.39	36.31	36.31	16.60	16.60
X	10.52	1000	118.98	154.96	23.59	23.59	10.78	10.78

* $\omega_n = \sqrt{\frac{K}{M_i + m + m_{added}}}$

Table 3. Added Mass Effects at *u*=0

1	The beam is vibrating in a viscous fluid enclosed by a rigid, concentric cylindrical shell.
2	The beam is cylindrical with a uniform cross section over its entire length.
3	The fluid boundary conditions are zero velocity at the outer shell and that the fluid velocity matches the beam velocity on the beam surface.
4	The length of the beam greatly exceeds its nominal diameter.
5	The beam is an isotropic linearly elastic solid.
6	Flow from the reservoir to the annulus does not disturb the annulus fluid at the location of interest.
7	The amplitude of vibration of the beam is far smaller than any length scale in the beam geometry.
8	The annulus fluid is assumed homogeneous, Newtonian, and incompressible.

Table A.1. Assumptions Used in Derivations

		Case													
		Axial Force Effects			Annulus Fluid Density				Inviscid System			Viscous System			
Variable	Units	I	II	III	IV	V	VI	VII	VIII	IX	X	XI	XII	XIII	XIV
E^*	kg/ms	0			0				0			0			
E	N/m^2	2E+11			2E+11				2E+11			2E+11			
d	m	0.06			0.06				0.06			0.06			
w_t	m	0.011			0.011				0.011			0.011			
I	m^4	5.65E-06			5.65E-06				5.65E-06			5.65E-06			
A_p	m^2	3.77E-03			3.77E-03				3.77E-03			3.77E-03			
A_i	m^2	7.54E-03			7.54E-03				7.54E-03			7.54E-03			
ν	-	0			0				0			0			
ρ_p	kg/m^3	7800			7800				7800			7800			
α	$1/K$	0			0				0			0			
m	kg/m	29.38			29.38				29.38			29.38			
g	m/s^2	9.81			9.81				9.81			9.81			
L	m	9			9				9			9			
L^e	m	4.5			4.5				4.5			4.5			
ρ_e	kg/m^3	0			0	3000	700	1000	0	1000		0	1000		
D	m	∞			NA**				∞	1.5d	1.1d	∞	1.1d	1.12d	1.1d
υ_e	m^2/s	0			NA**				0			0	1E-05	1E-04	
M_i	kg/m	6.6			6.6				6.6			6.6			
U	m/s	Varies*			0				Varies*			Varies*			
$\bar{T}$	N	1E+05	0	-2E+05	0				0			0			
$\bar{p}$	N/m^2	0			0				0			0			
ΔT	K	0			0				0			0			
c	kg/s	0			0				0			0			

**The flow velocity is taken to be negative, indicating flow in the direction opposite that shown in Figure 1.*

***Hydrodynamic function is hard coded to specified numeric values.*

Table B.1. Inputs Used in the Various Cases